ARTICLES

Spectroscopic Study of the Benchmark Mn^+-H_2 Complex

Viktoras Dryza, Berwyck L. J. Poad, and Evan J. Bieske*

School of Chemistry, The University of Melbourne, Victoria, Australia 3010

Received: April 6, 2009

We have recorded the rotationally resolved infrared spectrum of the weakly bound Mn^+-H_2 complex in the H−H stretch region (4022−4078 cm^{-1}) by monitoring Mn^+ photodissociation products. The band center of Mn^+-H_2, the H−H stretch transition, is shifted by −111.8 cm^{-1} from the transition of the free H_2 molecule. The spectroscopic data suggest that the Mn^+-H_2 complex consists of a slightly perturbed H_2 molecule attached to the Mn^+ ion in a T-shaped configuration with a vibrationally averaged intermolecular separation of 2.73 Å. Together with the measured $Mn^+\cdots H_2$ binding energy of 7.9 kJ/mol (Weis, P.; et al. *J. Phys. Chem. A* **1997**, *101*, 2809.), the spectroscopic parameters establish Mn^+-H_2 as the most thoroughly characterized transition-metal cation−dihydrogen complex and a benchmark for calibrating quantum chemical calculations on noncovalent systems involving open d-shell configurations. Such systems are of possible importance for hydrogen storage applications.

1. Introduction

Whereas hydrogen is an attractive candidate as a clean fuel for transport purposes, it has proved difficult to develop appropriate technologies for its efficient, safe, and economical storage.[1,2] Materials that bind intact dihydrogen molecules through weak physisorption interactions (∼10−50 kJ/mol) are attractive storage candidates because they are able to absorb and release H_2 rapidly and reversibly at low temperatures. Several materials containing transition-metal atoms have been suggested for this purpose. For example, transition-metal atoms integrated into carbon nanostructures are predicted to coordinate multiple dihydrogen molecules with electron donation from the metal atoms to the carbon nanostructure enhancing binding because of electrostatic interactions.[3−7] Metal−organic frameworks (MOF), microporous network materials consisting of metal atoms connected by bridging organic molecules, constitute another class of materials that can store hydrogen through physisorption. MOFs with exposed transition-metal atom sites are particularly promising because direct dihydrogen interactions at these oxidized sites are stronger than those at shielded sites.[8] Information on the interaction between the H_2 and the exposed metal atom has been obtained through infrared (IR) spectroscopy[9,10] and neutron scattering,[11−13] although the low thermal stability of some MOFs renders the latter technique almost unusable.[8]

Here we present a gas-phase spectroscopic study of the manganese cation−dihydrogen complex (Mn^+-H_2), a small, fundamental system that is appropriate for understanding the interaction between dihydrogen and a transition-metal cation. The rotationally resolved IR spectrum of Mn^+-H_2 is obtained in the H−H stretch region, with the analysis yielding accurate vibrational frequencies and structural parameters that are related to the strength of the metal-cation−dihydrogen bond. Although IR spectra for noncovalent molecular complexes containing open-shell transition-metal cations have previously been reported,[14,15] spectra exhibiting resolved rovibrational features, which allow bond distances to be extracted, are rare.

The spectroscopic data for Mn^+-H_2 can be used to gauge the efficacy of different computational approaches currently used to understand the H_2 interaction with metal atoms in carbon nanostructures and MOFs and to guide the rational development of new materials.[3−7,10,16−18] Computational exploration of the transition-metal atoms' role in hydrogen storage materials is usually performed using density functional theory (DFT). For reasonably large systems, the results obtained are similar to those from ab initio methods, yet they require substantially less computing time. Nonetheless, systems containing a transition-metal atoms are challenging subjects for DFT because of the number of electrons and bonding orbitals. Usually, effective core potentials and smaller d-orbital basis sets are employed to make the calculations viable (albeit less precise). DFT can also have difficulties in calculating the properties of systems with partially filled d-orbital configurations, with the results depending on which exchange and correlation functionals are implemented.[19] Moreover, DFT does not account for dispersion forces, which can play an important role in weak physisorption interactions.[20]

Before performing quantum chemical calculations on realistic hydrogen storage systems, the chosen computational method should preferably be calibrated using a smaller subsystem such as Mn^+-H_2 for which there are accurate experimental data, thereby engendering confidence in the computational approach and helping identify systematic errors.

Interactions between H_2 and the first-row transition-metal cations (M^+) have previously been explored experimentally through measurements of gas-phase clustering equilibria and theoretically through DFT calculations. (See ref 21 and references contained within.) As shown for Mn^+-H_2 in Figure 1, the M^+-H_2 complexes are predicted to have T-shaped structures, a configuration favored by the electrostatic charge−

* Corresponding author. E-mail: evanjb@unimelb.edu.au.

10.1021/jp9031767 CCC: $40.75
Published on Web 04/30/2009

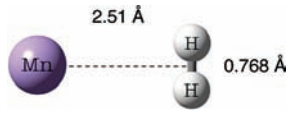

Figure 1. Calculated structure for Mn^+-H_2 taken from ref 22.

quadrupole interaction and by electron donor−acceptor bonding. The interaction between H_2 and Mn^+ in its ^7S ground electronic state (a $4s^13d^5$ configuration) is particularly weak ($D_0 \approx 7.9$ kJ/mol) because of Pauli repulsion between electrons in the large, singly occupied Mn^+ 4s orbital and the filled H_2 1σ orbital.[22] Although promotion of the 4s electron to give a $3d^6$ configuration would reduce this repulsion, the resulting ^5D state lies substantially higher in energy (1.82 eV).[23] In fact, the repulsion is ameliorated to some extent by partial hybridization of the 4s orbital with the higher energy $4p_z$ orbital, resulting in transfer of electron density away from the intermolecular region. Back bonding from the Mn^+ d_{yz} π orbital into the H_2 $2\sigma^*$ antibonding orbital does not contribute to the interaction because back donation from a half-filled d π orbital reduces d−d exchange stabilization energy.[22,24]

The weak nature of the $Mn^+\cdots H_2$ bond is evident from the structural parameters calculated using the B3LYP method and a split valence plus polarization (SVP) function basis set,[22] which predict an intermolecular bond length of 2.51 Å and an increase in the H−H bond length compared with the free H_2 molecule of only 0.002 Å. (See Figure 1.)

2. Experimental and Computational Approach

Conveniently, the weak intermolecular bond makes Mn^+-H_2 a suitable candidate for interrogation using IR photodissociation spectroscopy. This experimental approach relies on absorption of a single IR photon by the H_2 subunit with the deposited vibrational energy migrating into the weak intermolecular bond, which subsequently ruptures. Because the H−H stretch (ν_{HH}) frequency of Mn^+-H_2 is only slightly reduced compared with the free H_2 molecule (4161 cm^{-1}), excitation of this vibrational mode is sufficient to sever the weak $Mn^+\cdots H_2$ bond ($D_o \approx$ 660 cm^{-1}).[22]

The IR photodissociation experiments were conducted using a home-built tandem mass spectrometer that has been used for studies of other similar M^+-H_2 complexes (M = Li, B, Na, Mg, and Al).[25−30] Briefly, the Mn^+-H_2 complexes were generated by laser vaporization of a 4 mm diameter manganese rod adjacent to a supersonic expansion of pure H_2 gas. The central portion of the supersonic expansion was selected by a skimmer and passed into a quadrupole mass filter that was tuned to the mass of Mn^+-H_2. Next, the Mn^+-H_2 ions were turned 90° by an electrostatic bender into an octapole ion guide where they were overlapped with a counterpropagating IR beam originating from an optical parametric oscillator (Continuum Mirage 3000, 0.017 cm^{-1} bandwidth). The IR beam could be tuned over the 4000−4200 cm^{-1} range corresponding to the ν_{HH} region of the H_2 subunit. IR light that was resonant with a rovibrational ν_{HH} transition of Mn^+-H_2 caused the complex to break up into Mn^+ and H_2 fragments. A second quadrupole mass filter selected any resulting Mn^+ fragments, which passed to an ion detector. We obtained the IR spectrum by monitoring the Mn^+ photofragment intensity as a function of IR wavelength.

Complementary DFT calculations were performed using the Gaussian 03 computational software to determine the optimized geometry, binding energy, and harmonic vibrational frequencies of the Mn^+-H_2 complex.[31] For this investigation, the two hybrid DFT methods B3LYP and PBE1PBE were utilized. Ahlrich's triple-ζ valence plus polarization (TZVP) all-electron basis set was used for both the Mn and H atoms. Pure spherical harmonic functions were used with this basis set, and the calculations were performed on a large grid of size (99, 590). The purpose of the present computational investigation is to determine how well the Mn^+-H_2 complex is described by DFT methods with basis sets commonly applied to investigate larger hydrogen storage systems. Although ab initio calculations with very large basis sets are computationally viable on small systems such as Mn^+-H_2, they are currently not feasible for larger model systems used to replicate hydrogen storage materials.

For each DFT method, the calculated ν_{HH} frequency of Mn^+-H_2 was scaled by the factor required to reconcile the calculated ν_{HH} frequency of the free H_2 molecule with the experimental value (scaling factor of 0.9405 for B3LYP/TZVP and 0.9418 for PBE1PBE/TZVP). The ν_{HH} frequency of Mn^+-H_2 calculated by Bowers and coworkers[22] was adjusted in a similar way (scaling factor 0.9533). Corrections to the calculated binding energies due to zero-point energies and basis set superposition effects were included.

3. Results and Discussion

3.1. Analysis of the Infrared Spectrum. The Mn^+-H_2 complex is anticipated to be a near-prolate asymmetric rotor because the moments of inertia about the *B* and *C* axes are almost equal and are much larger than the moment of inertia about the *A* axis (i.e., the intermolecular axis).[22] Excitation of the ν_{HH} mode causes a dipole moment change along the intermolecular axis, resulting in rovibrational transitions that are characteristic of a parallel A-type band. The transition selection rules are $\Delta K_a = 0$ and $\Delta K_c = \pm 1$, where K_a and K_c are the projections of the rotational angular momentum ($\hat{N}$) along the *A* and *C* axes, respectively. The selection rules for the rotational angular momentum are $\Delta N = 0, \pm 1$ ($\Delta N = \pm 1$) for the $K_a > 0$ ($K_a = 0$) states. The rotational angular momentum ($\hat{N}$) and electronic spin ($\hat{S}$) are related to the total angular momentum (excluding nuclear spin) by $\hat{J} = \hat{N} + \hat{S}$. Transition selection rules for the total angular momentum excluding nuclear spin are $\Delta J = 0, \pm 1$ ($\Delta J = \pm 1$) for the $K_a > 0$ ($K_a = 0$) states. Although each *N* level is associated with 7 *J* sublevels, the spectral structure associated with spin-rotation splitting is not resolved in this study so that the observed transitions can be assigned in terms of *N*, K_a, and K_c.

The Mn^+-H_2 IR spectrum in the 4022−4078 cm^{-1} ν_{HH} region (Figure 2) displays full rotational resolution and has an appearance that is compatible with the predicted T-shaped C_{2v} structure of the complex (Figure 1). Only $K_a = 1-1$ sub-band transitions, associated with complexes containing the ortho modification of H_2, have significant intensity. The predominance of complexes containing the ortho form (i.e., odd K_a) over those containing the para form (i.e., even K_a) is expected; as for normal H_2 gas, the ortho/para ratio is 3:1. Furthermore, Mn^+-H_2 (para) complexes are rapidly converted to the more stable Mn^+-H_2 (ortho) complexes through exothermic ligand switching reactions in the ion source.[27,32]

The $K_a = 1-1$ sub-band displays a P branch ($\Delta N = -1$), Q branch ($\Delta N = 0$), and R branch ($\Delta N = +1$), as labeled in Figure 2. The peaks in the P and R branches appear as doublets because of asymmetry splitting (i.e., $\Delta K_c = \pm 1$). Each peak of the doublet should consist of seven overlapping subcomponent transitions corresponding to the different possible values of *J* for each value of *N*. Although these subcomponent transitions are unresolved, they may contribute to the widths of the observed lines (fwhm $\simeq$ 0.07 cm^{-1}). Other possible contributions

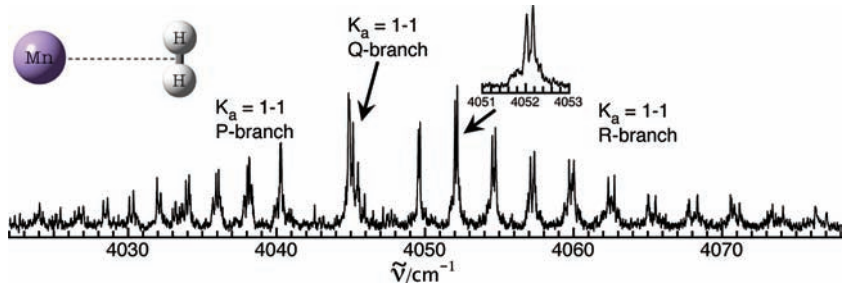

Figure 2. Infrared spectrum of Mn^+-H_2 in the H−H stretch region obtained by monitoring Mn^+ photofragments. The P, Q, and R branches of the $K_a = 1-1$ sub-band are labeled.

TABLE 1: Spectroscopic Constants for Mn^+-H_2 Derived by Fitting the ν_{HH} $K_a = 1-1$ Transitions to a Watson *A*-Reduced Hamiltonian[a]

	exptl		calcd		
	$n_{HH} = 0$	$n_{HH} = 1$	B3LYP/SVP[b]	B3LYP/TZVP[c]	PBE1PBE/TZVP[d]
B	1.1752(12)	1.2082(12)			
C	1.1296(12)	1.1597(12)			
$\bar{B}$	1.1524(12)	1.1839(12)			
$\Delta_J \times 10^4$	1.48(10)	1.36(10)			
ν_{sub}[e]	4044.85(1)				
ν_{HH}[f]	4049.4(1.5)		4059	4037	4036
$\Delta\nu_{HH}$[f]	−111.8(1.5)		−102	−124	−125
R/Å[g]	2.73	2.69	2.51	2.57	2.56
ω_s	203	221	320	296	299
ω_b			391	369	391
D_0[h]	660(140)		890	538	570

[a] Unless otherwise indicated, units are cm^{-1}. For each value, the error in the last significant figure(s) is given in parentheses. Calculated DFT values are also given. [b] Calculated values from ref 22. [c] B3LYP with Ahlrich's triple-ζ valence plus polarization (TZVP) all-electron basis. [d] PBE1PBE with Ahlrich's triple-ζ valence plus polarization (TZVP) all-electron basis. [e] Sub-band origin for $K_a = 1-1$ transitions. [f] DFT ν_{HH} and $\Delta\nu_{HH}$ values are scaled by the factors required to reconcile calculated and measured H_2 stretch frequencies. (See the text.) [g] Experimental data are vibrationally averaged separations (R_0), whereas calculated values are equilibrium separations (R_e). [h] Experimental D_0 from ref 22.

to the line-widths include lifetime broadening of the excited vibrational state due to coupling with the $Mn^+ + H_2$ dissociation continuum, power broadening, and a 0.017 cm^{-1} contribution from the IR bandwidth.

The $K_a = 1-1$ sub-band transitions were fitted to an *A*-reduced Watson Hamiltonian yielding the spectroscopic parameters presented in Table 1. The ground- and excited-state *A* rotational constants cannot be determined from a parallel A-type band because the fits A'' and A' were constrained to the rotational constant of the free H_2 molecule in the ground vibrational state ($B'' = 59.33$ cm^{-1}).[33] The ν_{HH} band center is expected to lie between ΔB and $2\Delta B$ higher in energy than the $K_a = 1-1$ sub-band center (4044.9 cm^{-1}), where $\Delta B = B'' - B' \simeq 3$ cm^{-1} is the difference between the rotational constant of the free H_2 molecule in its ground and excited vibrational states.[33] The two limits are based on the Mn^+-H_2 complex being either a rigid T-shaped rotor or, alternatively, exhibiting free internal rotation of the H_2 subunit. Because the actual situation will lie between these two extremes, the ν_{HH} band center is deemed to be the average of the two limits, that is, 4049.4 ± 1.5 cm^{-1}. This implies that the transition is displaced by −111.8 cm^{-1} from the Q_1 (0) transition of the free H_2 molecule (4161.2 cm^{-1}).[33]

The vibrationally averaged intermolecular $Mn^+\cdots H_2$ separation estimated from $\bar{B} = (B + C)/2$ is 2.73 Å, contracting by 0.04 Å upon vibrational excitation of the H_2 subunit. The contraction is presumably due to an increase in the vibrationally averaged polarizability and quadrupole moment of the H_2 molecule leading to an enhancement of the electrostatic and induction interactions.[34] The equilibrium $Mn^+\cdots H_2$ separation is not immediately derivable from the vibrationally averaged intermolecular separation. However, comparisons with Na^+-H_2, which has a binding energy and intermolecular bond length similar to those of Mn^+-H_2, and for which an accurate potential energy surface has been constructed and used to calculate rovibrational energy levels suggest that the equilibrium separation should be around 0.1 Å less than the vibrationally averaged value (i.e., ∼2.63 Å).[28]

Because of the weak intermolecular bond and large rotational constant of the H_2 subunit, the Mn^+-H_2 complex is expected to exhibit considerable zero-point motion in the bending vibration coordinate. This floppiness is manifested in an exaggerated difference between the *B* and *C* constants compared with a rigid T-shaped structure.[35] Consequently the inertial defect $1/C - 1/B - 1/A$ is not zero (as it would be for a rigid planar molecule) so that the *A* constant and the H−H bond distance cannot be determined from *B* and *C*.

3.2. Density Functional Theory Calculations. In this section, we briefly compare the measured properties of Mn^+-H_2 with the results of previous B3LYP/SVP and current B3LYP/TZVP and PBE1PBE/TZVP DFT calculations, with particular reference to the dissociation energy, the intermolecular separation, the harmonic intermolecular stretching frequency, and the stretching frequency of the H_2 subunit.

At the outset, it is worthwhile to recall that Mn^+-H_2 is a weakly bound complex that exhibits large-amplitude, zero-point excursions in the intermolecular stretch and bend vibrational coordinates (even when the complex is in its ground vibrational state). There are several consequences of this floppiness. First, the intermolecular vibrational modes will probably have frequencies lower than the DFT harmonic estimates. Therefore, the calculated dissociation energy, D_0, estimated using a zero-point energy calculated from the harmonic vibrational frequencies, will tend to underestimate the actual binding energy. Second, because of zero-point vibrational excursions (particularly in the *R* coordinate), the calculated intermolecular separation, R_e, is likely to be less than the vibrationally averaged separation, R_0, deduced from the rotational constants. Third, because of stretch−bend coupling, the harmonic stretching frequency estimated from the rotational and centrifugal distortion constants will probably be lower than the ab initio estimate (which is related to the second derivative of the potential energy along the *R* coordinate at the PES minimum). Even in the ground vibrational state, the complex undergoes large-amplitude bending excursions, sampling regions of the PES where the $Mn^+\cdots H_2$ radial attraction is weaker than it is in the T-shaped

equilibrium configuration. This reduces the effective radial force constant, causing the experimental ω_s value to be less than the DFT harmonic estimate.

Eventually, making full contact between experiment and theory requires the development of a 3D PES that is subsequently used to calculate the rovibrational energies of the complex. This procedure has not yet been accomplished for Mn^+-H_2 but has been accomplished for the Na^+-H_2 complex, which has a similar binding energy (660 and 860 cm^{-1}, respectively).[28] Therefore, the findings for Na^+-H_2 should provide a guide for Mn^+-H_2.

The experimental and DFT data for Mn^+-H_2 are summarized in Table 1. From the experimental $\bar{B}$ value, one can deduce a vibrationally averaged intermolecular separation ($R_0 = 2.73$ Å) that is 0.22, 0.16, and 0.17 Å greater than the equilibrium separations predicted, respectively, by the B3LYP/SVP, B3LYP/TZVP and PBE1PBE/TZVP levels. For Na^+-H_2, the vibrationally averaged separation, R_0, exceeds the equilibrium separation, R_e, by ~0.1 Å, and it seems likely that R_0 exceeds R_e by a similar amount in Mn^+-H_2. This would imply that the B3LYP/TZVP and PBE1PBE/TZVP levels do a reasonable job of predicting the equilibrium intermolecular separation. The experimental ω_s value (203 cm^{-1}) is around 30% lower than the DFT estimates (320, 296, and 299 cm^{-1} for B3LYP/SVP, B3LYP/TZVP, and PBE1PBE/TZVP levels). A similar reduction (~20%) for the experimental ω_s value compared with the ab initio harmonic estimate was found for Na^+-H_2 because of stretch−bend coupling.

The harmonic bending frequencies (ω_b) calculated using the B3LYP/SVP, B3LYP/TZVP and PBE1PBE/TZVP DFT levels (391, 369, and 391 cm^{-1}, respectively) are comparable to the calculated barrier for internal rotation of the H_2 subunit (402 and 453 cm^{-1} at the B3LYP/TZVP and PBE1PBE/TZVP levels) and therefore obviously overestimate the actual bending frequency.

In general, the B3LYP/SVP, B3LYP/TZVP and PBE1PBE/TZVP DFT levels all do a reasonable job of estimating the experimental ν_{HH} frequency (4049.4 cm^{-1}). One derives scaled frequencies of 4059, 4037, and 4036 cm^{-1}, respectively, if the harmonic DFT frequencies are scaled by the appropriate factor so that the method reproduces the frequency of the bare H_2 molecule.

As far as the binding energy is concerned, the experimental value (660 ± 140 cm^{-1}) is underestimated by the B3LYP/TZVP and PBE1PBE/TZVP levels (538 and 570 cm^{-1}, respectively) and overestimated by the B3LYP/SVP level (890 cm^{-1}). As explained above, because of an overestimation of the two intermolecular vibrational modes' frequencies, the DFT dissociation energy is likely to underestimate the actual value (as is the case for the B3LYP/TZVP and PBE1PBE/TZVP levels). Compared with Na^+-H_2, for which the difference is 8%, the discrepancy is larger for Mn^+-H_2 (18 and 14% for the B3LYP/TZVP and PBE1PBE/TZVP levels), perhaps because Mn^+-H_2 is more weakly bound than Na^+-H_2 and the two intermolecular modes are more anharmonic.

In summary, the B3LYP/TZVP and PBE1PBE/TZVP levels appear to give reasonable descriptions of the Mn^+-H_2 complex regarding the binding energy, the intermolecular bond length, and the intermolecular stretch frequency. The B3LYP/SVP level used by Bowers and coworkers overestimates the binding energy and may also underestimate the intermolecular separation slightly.

3.3. Comparisons with Related Complexes. The $\Delta\nu_{HH}$ vibrational shift for ion complexes containing H_2 is sometimes presumed to be linearly correlated with the binding energy (D_0).[41,42] Therefore, it is interesting to compare $\Delta\nu_{HH}$ and D_0 for Mn^+-H_2 with corresponding values for the Li^+-H_2, B^+-H_2, Na^+-H_2, Mg^+-H_2, and Al^+-H_2 complexes that have also been studied spectroscopically,[26−30] theoretically,[39,40] and thermochemically.[22,36−38] In general, complexes containing the Mn^+, B^+, Mg^+, and Al^+ cations, which have a singly or doubly occupied valence s orbital, exhibit a larger $\Delta\nu_{HH}$ red shift for a given dissociation energy than complexes containing the Li^+ and Na^+ cations. The trends are apparent in Figure 3 where $\Delta\nu_{HH}$ is plotted against D_0; data for complexes containing cations with a half-filled or filled valence s orbital (B^+, Mg^+, Al^+, and Mn^+) and data for complexes containing alkali metal cations (Li^+, Na^+) lie on separate lines. In general, the large $\Delta\nu_{HH}$ shifts for complexes containing B^+, Mg^+, Al^+, and Mn^+ can be linked to hybridization of the valence s orbital on the metal cation with a low-lying p_z orbital directed toward the hydrogen molecule facilitating charge transfer from the H_2 σ_g bonding orbital to a metal-centered sp hybrid orbital, thereby weakening the H−H bond.[27]

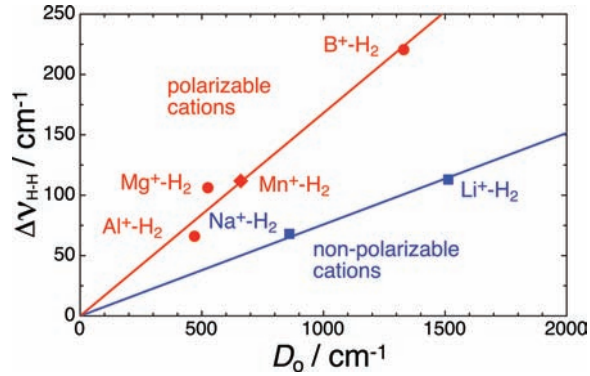

Figure 3. Frequency shift for the H−H stretch vibration ($\Delta\nu_{HH}$) plotted against dissociation energy (D_0) for M^+-H_2 complexes (M = Li, B, Na, Mg, Al, and Mn). The plotted data are experimental values (from refs 22, 26−30 and 36−38) apart from the D_0 values of Li^+-H_2 and Mg^+-H_2, which are calculated values taken from refs 39 and 40, respectively.

4. Concluding Remarks

In summary, the rotationally resolved IR spectrum of Mn^+-H_2 has been obtained in the H−H stretch region using photodissociation spectroscopy. Properties extracted from the spectrum include the vibrationally averaged intermolecular bond length ($R_0 = 2.73$ Å), the H−H stretch frequency red shift ($\Delta\nu_{HH} = -111.8$ cm^{-1}), and an estimate for the harmonic intermolecular stretch frequency ($\omega_s = 203$ cm^{-1}). These data, together with the previously determined H_2 binding energy ($D_o = 660$ cm^{-1}),[22] establish Mn^+-H_2 as a robust benchmark for calibrating ab initio and DFT calculations on systems involving open d-shell configurations and weak physisorption interactions. Ultimately, a proper theoretical description of the Mn^+-H_2 complex and full comparison with the spectroscopic data will require calculation of a 3D potential energy surface, followed by rovibrational energy level calculations. This approach, as accomplished recently for Na^+-H_2 and Al^+-H_2,[28,30] allows direct comparisons between the calculated and measured transition energies and provides a critical test of the computed interaction potential energy surface.

Acknowledgment. We are grateful to the Australian Research Council and the University of Melbourne for supporting this research.

Supporting Information Available: Transition wavenumbers and assignments along with the full citation for ref 31.

This material is available free of charge via the Internet at http://pubs.acs.org.

References and Notes

(1) Schlapbach, L.; Zuttel, A. *Nature* **2001**, *414*, 353–358.
(2) van den Berg, A. W. C.; Otero Areán, C. *Chem. Commun.* **2008**, 668–681.
(3) Zhao, Y. F.; Kim, Y. H.; Dillon, A. C.; Heben, M. J.; Zhang, S. B. *Phys. Rev. Lett.* **2005**, *94*, 155504.
(4) Yildirim, T.; Ciraci, S. *Phys. Rev. Lett.* **2005**, *94*, 175501.
(5) Sun, O.; Wang, Q.; Jena, P.; Kawazoe, Y. *J. Am. Chem. Soc.* **2005**, *127*, 14582–14583.
(6) Durgun, E.; Ciraci, S.; Yildirim, T. *Phys. Rev. B* **2008**, *77*, 085405.
(7) Kim, G.; Jhi, S. H.; Park, N.; Louie, S. G.; Cohen, M. L. *Phys. Rev. B* **2008**, *78*, 085408.
(8) Dinca, M.; Long, J. R. *Angew. Chem., Int. Ed.* **2008**, *47*, 6766–6779.
(9) Prestipino, C.; Regli, L.; Vitillo, J. G.; Bonino, F.; Damin, A.; Lamberti, C.; Zecchina, A.; Solari, P. L.; Kongshaug, K. O.; Bordiga, S. *Chem. Mater.* **2006**, *18*, 1337–1346.
(10) Vitillo, J. G.; Regli, L.; Chavan, S.; Ricchiardi, G.; Spoto, G.; Dietzel, P. D. C.; Bordiga, S.; Zecchina, A. *J. Am. Chem. Soc.* **2008**, *130*, 8386–8396.
(11) Peterson, V. K.; Liu, Y.; Brown, C. M.; Kepert, C. J. *J. Am. Chem. Soc.* **2006**, *128*, 15578–15579.
(12) Dinca, M.; Dailly, A.; Liu, Y.; Brown, C. M.; Neumann, D. A.; Long, J. R. *J. Am. Chem. Soc.* **2006**, *128*, 16876–16883.
(13) Liu, Y.; Kabbour, H.; Brown, C. M.; Neumann, D. A.; Ahn, C. C. *Langmuir* **2008**, *24*, 4772–4777.
(14) Duncan, M. A. *Int. Rev. Phys. Chem.* **2003**, *22*, 407–435.
(15) MacAleese, L.; Maitre, P. *Mass Spectrom. Rev.* **2007**, *26*, 583–605.
(16) Yang, Q. Y.; Zhong, C. L. *J. Phys. Chem. B* **2006**, *110*, 655–658.
(17) Sun, Y. Y.; Kim, Y. H.; Zhang, S. B. *J. Am. Chem. Soc.* **2007**, *129*, 12606–12607.
(18) Zhou, W.; Yildirim, T. *J. Phys. Chem. C* **2008**, *112*, 8132–8135.
(19) Weinert, M.; Watson, R. E.; Fernando, G. W. *Phys. Rev. A* **2002**, *66*, 032508.
(20) Wu, X.; Vargas, M. C.; Nayak, S.; Lotrich, V.; Scoles, G. *J. Chem. Phys.* **2001**, *115*, 8748–8757.
(21) Kemper, P. R.; Weis, P.; Bowers, M. T.; Maitre, P. *J. Am. Chem. Soc.* **1998**, *120*, 13494–13502.
(22) Weis, P.; Kemper, P. R.; Bowers, M. T. *J. Phys. Chem. A* **1997**, *101*, 2809–2816.
(23) Moore, C. E. *Atomic Energy Levels As Derived from the Analyses of Optical Spectra*; U.S. National Bureau of Standards: Washington, DC, 1971; Vol. 35.
(24) Kemper, P. R.; Weis, P.; Bowers, M. T. *Int. J. Mass Spectrom. Ion Processes* **1997**, *160*, 17–37.
(25) Thompson, C.; Emmeluth, C.; Poad, B.; Weddle, G.; Bieske, E. *J. Chem. Phys.* **2006**, *125*, 044310–044315.
(26) Emmeluth, C.; Poad, B. L. J.; Thompson, C. D.; Weddle, G. H.; Bieske, E. J. *J. Chem. Phys.* **2007**, *126*, 204309.
(27) Dryza, V.; Poad, B. L. J.; Bieske, E. J. *J. Am. Chem. Soc.* **2008**, *130*, 12986–12991.
(28) Poad, B. L. J.; Wearne, P. J.; Bieske, E. J.; Buchachenko, A. A.; Bennett, D. I. G.; Klos, J.; Alexander, M. H. *J. Chem. Phys.* **2008**, *129*, 184306–184308.
(29) Dryza, V.; Poad, B. L.; Bieske, E. J. *J. Phys. Chem. A* **2009**, *113*, 199–204.
(30) Emmeluth, C.; Poad, B. L. J.; Thompson, C. D.; Weddle, G. H.; Bieske, E. J.; Buchachenko, A. A.; Grinev, T. A.; Kłos, J. *J. Chem. Phys.* **2007**, *127*, 164310.
(31) Frisch, M. J.; et al. *Gaussian 03*, revision D.01; 2005. The full reference is given in the Supporting Information.
(32) Lovejoy, C.; Nelson, D.; Nesbitt, D. J. *J. Chem. Phys.* **1987**, *87*, 5621–5628.
(33) Bragg, S. L.; Brault, J. W.; Smith, W. H. *Astrophys. J.* **1982**, *263*, 999–1004.
(34) Hunt, J. L.; Poll, J. D.; Wolniewicz, L. *Can. J. Phys.* **1984**, *62*, 1719–1723.
(35) Nesbitt, D. J.; Naaman, R. *J. Chem. Phys.* **1989**, *91*, 3801.
(36) Kemper, P. R.; Bushnell, J. E.; Weis, P.; Bowers, M. T. *J. Am. Chem. Soc.* **1998**, *120*, 7577.
(37) Bushnell, J. E.; Kemper, P. R.; Bowers, M. T. *J. Phys. Chem.* **1994**, *98*, 2044–2049.
(38) Kemper, P. R.; Bushnell, J.; Bowers, M. T.; Gellene, G. I. *J. Phys. Chem.* **1998**, *102*, 8590–8597.
(39) Kraemer, W. P.; Špirko, V. *Chem. Phys.* **2006**, *330*, 190–203.
(40) Bauschlicher, C. W. *Chem. Phys. Lett.* **1993**, *201*, 11–14.
(41) Olkhov, R. V.; Nizkorodov, S. A.; Dopfer, O. *J. Chem. Phys.* **1997**, *107*, 8229–8238.
(42) Vitillo, J. G.; Damin, A.; Zecchina, A.; Ricchiardi, G. *J. Chem. Phys.* **2005**, *122*, 114311/1–114311/10.

JP9031767